J.M. LACKNER*#, B. MAJOR**, W. WALDHAUSER*, A. MZYK*,**, Ł. MAJOR**, M. KOT***

ROUGHNESS INFLUENCE ON MACRO- AND MICRO-TRIBOLOGY OF MULTI-LAYERED HARD COATINGS ON CARBON FIBRE POLYMER COMPOSITE

WPŁYW CHROPOWATOŚCI NA MAKRO- I MIKRO-TRIBOLOGIĘ WIELOWARSTWOWYCH TWARDYCH POWŁOK NA BAZIE ZBROJONYCH WŁÓKNAMI KOMPOZYTÓW POLIMEROWYCH

Goal of this work is the investigation of roughness influences on the abrasive wear behaviour of magnetron sputtered multi-layered, low-friction coatings on carbon-fibre reinforced polymers (CFRP). Higher coating roughness at similar CFRP quality was realized by higher deposition rates, leading to increased heat flux to the substrates during deposition. Thermal expansion of the epoxy matrix on the micro scale results in a wavy, wrinkled surface topography. Both in scratch and reciprocal sliding testing against alumina, the friction coefficients are lower for the smooth coatings, but their wear rate is higher due to low-cycle fatigue caused abrasion.

Keywords: carbon fibre reinforced polymers, hard coatings, multi-layer, roughness, tribology

Celem pracy jest badanie wpływów szorstkości na zużycia abrazyjne osadzonych magnetronowo wielowarstwowych powłoki o niskim współczynniku tarcia na bazie wzmocnionych włóknami węglowych polimerów (CFRP). Większa szorstkość powłoki przy podobnej jakości (CFRP) została uzyskana przez wyższe szybkości osadzania, co prowadziło do zwiększonego strumienia ciepła do podłoża podczas osadzania. Rozszerzalność cieplna matrycy epoksydowej w skali mikro pozwalała na uzyskanie falistej, pofałdowanej topografii powierzchni. Zarówno w teście zarysowania jak i ścierania z przeciwpróbką korundową uzyskano niższe współczynniki tarcia dla gładkich powierzchni zaś ich szybkość zużycia była wyższa ze względu na nisko-cyklowe zmęczenie wywołujace przetarcie.

1. Introduction

Carbon-fibre reinforced polymer composite (CFRP) materials consist of endless carbon fibres in a polymer matrix (mostly epoxy resins), enabling the combination of very low density with extreme tensile strength for light-weight design. Nevertheless, the mechanical properties of CFRP are highly dependent on the fibre direction with 2000 MPa tensile strength and 140 GPa elastic modulus in fibre direction and only 70 MPa strength and 12 GPa elastic modulus in normal direction. More homogenous mechanical behaviour is reached by a composite design with multi-axial fibre direction.

To functionalize the surface of CFRP, a large variety of coating techniques were investigated in past. Besides decorative finishing with only low demands on scratch resistance, advanced applications of CFRP in mechanical engineering require durable tribological protection. Organic dip and spray coatings fail due to their softness. Plasma sprayed coatings (e.g. zirconia, alumina) are a hard material alternative, but struggle with fracture and delamination due to their high brittleness on soft, elastically deformable CFRP [1,2]. Similar problems arise for thicker galvanic coatings based on copper-nickel-chromium processes [3] and for hard physical vapour deposited coatings (e.g. plasma-polymerized oxynitride coatings) [4]. For both thin and brittle coatings, the varying surface elasticity on the micro scale due to different depth of carbon fibres. Reasonably, varying epoxy thickness above the fibres is a huge challenge for both thin and brittle coatings [5] to prevent cohesion fracture during loading. Besides low modulus

*   JOANNEUM RESEARCH FORSCHUNGSGES.M.B.H. INSTITUTE OF SURFACE TECHNOLOGIES AND PHOTONICS, FUNCTIONAL SURFACES WORKGROUP, LEOBNER STRASSE 94, 8712 NIKLASDORF, AUSTRIA
**   POLISH ACADEMY OF SCIENCES, INSTITUTE OF METALLURGY AND MATERIALS SCIENCES, UL. REYMONTA 25, 30-059 KRAKOW, POLAND
***   AGH UNIVERSITY OF SCIENCE AND TECHNOLOGY, FACULTY OF MECHANICAL ENGINEERING AND ROBOTICS, LABORATORY OF TRIBOLOGY AND SURFACE ENGINEERING, AL. A. MICKIEWICZA 30, 30-059 KRAKOW, POLAND

Corresponding author: Juergen.Lackner@joanneum.at

of the epoxy matrix, the thermal expansion coefficient is 15 times higher, which results in in similar higher deformation of uniaxial reinforced bars normal to the reinforcement. Under multi-axial reinforcement, expansion is only possible on the micro scale in the epoxy matrix between the fibres, resulting in micro-scale thermal-induced wrinkling phenomena at the surface in areas with large epoxy thickness. If such a composite is coated, wrinkling of the epoxy matrix leads to high local tensile strains in the coating on the micro scale with risk to fracture [6,7].

Local bending deformation of the soft epoxy matrix occurs under high tribological point loading too, as recently shown in own works for magnetron sputtered coatings [8]. Single-layered coatings fail by cohesive cracking through the whole thickness with a crack start at the surface or the interface depending on the type of bending. In coated multi-layered coatings consisting of hard, brittle and soft, deformable layers provide a very strong crack arrest mechanism [9]. Instead of the through-thickness fracture, only local fracture within the hard phase layers occurs in regions of too high stresses, while plastic deformation along the 45° planes in the soft layers in between dissipates energy. As a result, the coating shows no total failure, but only the formation of deformation bands, which are tilted towards the substrate depending on the hard-soft phase thickness ratio [9]. We presented such results recently for titanium-titanium nitride, chromium-chromium nitride ($Cr-Cr_2N$) and other multilayer systems [8,9]. The micro-scale deformation mechanism within the deformation bands comprises strain hardening and broadening of the deformation under too high loads instead of fracture [9].

Tribological stressed sliding surfaces gain for low friction coefficients. Low friction decreases the shear load in the coating (and substrate) during the tribological contact, which decreases the total coating stress (e.g. calculated based on the von-Mises assumption). Diamond-like carbon (DLC) coatings are such a class of amorphous carbon-based materials with a mixture of sp^2 and sp^3 hybridized carbon atoms, combining hardness properties of diamond with low-friction behaviour of graphite. While hydrogen-free DLC coatings (a-C) possess very high hardness, the toughness of these coatings increases with higher hydrogen content (a-C:H coatings) [10-13]. Doping with metals, forming carbides in the amorphous a-C:H matrix, increases deformability of the coatings, but also the friction coefficient [14-18]. Gradient or multilayer coating architectures may combine toughness, hardness and low-friction, based on above described biomimetic multilayer shear deformation mechanisms. Nevertheless, thicker DLC coatings on polymer surfaces for harsh tribological applications are scarcely realized yet.

The current work focusses on the influence of roughness of tribologically protective coatings on CFRP. Therefore, multi-layered $Cr-Cr_2N$ coatings with chemically-graded Cr-doped DLC top layers (a-C:H:Cr) with non-doped a-C:H surface were deposited onto CFRP. Modifications of the deposition condition resulted in different surface roughness. Scratch-tests and tribological testing was performed in order to investigate the fracture mechanisms under high point loads and low-cycle fatigue conditions for 2 different roughness conditions.

2. Experimental details

Coating deposition occurred by unbalanced DC pulsed magnetron sputtering. The load-bearing, multi-layered $Cr-Cr_2N$ base coating was deposited after ion plasma pre-treatment on the substrate, followed by the tribological functional, low-friction top coating (graded a-C:H:(Cr)). Prior deposition, the substrates (3 mm thick carbon-fibre reinforced epoxy-matrix polymers, Secar Technologie Ges.m.b.H., Hönigsberg, Austria) were cleaned in an industrial washing machine (Miele, Guetersloh, Germany) with surfactant washing agents, then dried and mounted on the 3D roTABLE planetary in the industrial-like R&D deposition equipment (Leybold Vakuum, Cologne, Germany). After pumping to high vacuum conditions (2×10^{-5} mbar), the ion plasma treatment was performed on substrates at room temperature without prior heating. Therefore, we used a linear anode layer ion source (Veeco ALS 340, Fort Collins, CO, USA) with oxygen-argon gas mixtures [19]. Subsequent $Cr-Cr_2N$ multi-layer deposition of the base coating occurred by 2 oppositely arranged rectangular sputter magnetrons, equipped with chromium targets (RHP Technologies, Seibersdorf, Austria) in Ar and $Ar-N_2$ gas flow. After finalizing deposition of 32 bilayers of $Cr-Cr_2N$ (~4.5 μm film thickness), the top layer coating deposition started from 2 Cr and 2 C targets (Schunk Elektrokohle, Bad Goisern, Austria). The C targets are placed in 90° position to the Cr targets in the chamber. During top layer deposition, we applied gas flows of C_2H_2 and Ar. ~1.5 μm thick gradient layers were realized by step-wise change of power and gas flow: The deposition started at high power on the Cr targets, which were sputtered in $Ar-C_2H_2$ atmosphere (10% C_2H_2). While the C_2H_2 percentage in the gas mixture and the sputter power on the Cr target decreased gradually, the sputter power on the 2 C targets increased. The last 1/3 of the film thickness was realized by pure C deposition in Ar atmosphere. The different roughness was realized by modifying the average deposition rate: Higher rate lead to the rougher coatings, while lower rate (~2/3) decreased the heat flux to the CFRP during deposition, resulting in ~81 and 61°C substrate temperature, respectively, at the end of deposition when reaching the desired thickness.

Roughness and coating thickness measurements on masked steps were done on a Veeco Dektak 150 (Santa Barbara, CA, USA) with a 2 μm diamond tip. Arithmetic roughness (Ra), geometric roughness (Rq = root-mean-square / RMS roughness), and the mean roughness depth (Rz) were analysed by Veeco's "Vision" software package based on EN ISO 25178 standards. Hardness and elastic modulus measurements occurred on an Anton-Paar / CSM-Instruments Nano-Hardness-Tester (Peseux, CH) with 2 mN loading of a Vickers indenter. The standard Oliver-Pharr method was used to calculate micromechanical properties from the load-depth curves.

The tribological testing was done on an Anton-Paar / CSM-Instruments Micro-Scratch-Tester (Peseux, CH) at ~55% relative humidity and 24°C. For scratch testing, a 100 μm radius HRC Rockwell diamond was applied, whereby the loading occurred

from 0.03 to 30 N on the 8 mm long scratch track at 8 mm/min scratching speed. A pre-scan was performed to obtain the initial surface topography. The indentation depth was recorded during scratching, presenting the elasto-plastic deformation (P_d), while the post-scan enabled the calculation of the pure plastic deformation (R_d) within the scratch track. Acoustic emission was additionally used for estimation of the critical loads (L_{c1} for first fracture through the coating and L_{c2} for first delamination from the CFRP). Tribological testing on this device used the possibility of pre- and post-scan as well as on-line depth measurement during sliding too, whereby the residual depth (pure plastic deformation) let us quantify the wear. 100 cycles linear reciprocal sliding occurred under 5 N loads, 1000 cycles under 2 N loading, whereby 6 mm diameter alumina balls were used. At the end of the sliding track, the ball was not unloaded but immediately accelerated in opposite direction. All measurements were done at least 5 times to achieve significant statistics. Given values are averages with a standard deviation of maximum 3% of the average for roughness and coating thickness, 5% for hardness and elastic modulus, and 6% for friction coefficient and wear track depth.

The micro- and nanostructure as well as fracture of the coatings were analysed by the application of transmission electron microscopy (TEM, TECNAI G2 F20 (200 kV FEG)) after focused ion beam (FIB) based cross-section sample preparation (Quanta 200 3D DualBeam microscope equipped with in-situ OmniProbe micro manipulator, gallium ions for milling). Electron diffraction patterns in high resolution mode were used for structural analyses, while the bright field technique was applied for imaging of the coating architecture and of tribological fracture behaviour and mechanisms.

3. Results and discussion

Table 1 shows the overview on film thickness, roughness, hardness and elastic modulus of both coating types. In general, the achieved total thickness and elastic modulus are quite similar for both types. Hardness slightly increases by ~5.5%, Ra, Rq and Rz decreases by 10.7, 18.4, and 23.3% for the smoother type. Compared to the roughness values for similar coatings on silicon wafers (Ra values in the 10's of nanometer), the drastically higher values are due to both rough, uncoated CFRP surfaces (Ra ~500-600 nm) plus a more than 50% increase by substrate heating and wrinkling effects, as shortly described in the introduction [7]: Increasing expansion of the epoxy matrix in between the fibres starting from the early film growth stages leads to wrinkling on the sub-micrometre scale ("nano-wrinkling"), which is visible in the coarse surface structure, e.g. in the light microscopy images outside the scratch tracks: The dots on the rougher coating surface (Fig. 1 c,d), deposited at ~20°C higher surface temperature at the end of deposition, represent individual small growth cones with distinct growth direction, which are missing in Fig. 1e,f for the smoother coating. The larger black dots are pores in the CFRP surface and have similar density on both surfaces (compare Fig. 1c and e). However, this sub-micrometer wrinkling is mechanically limited by stiffening of the surface by the growing film thickness, which either may crack or enlarge the wrinkle wavelength for stress release (see detailed explanations in [20]). Most of formed cracks are able to heal during ongoing deposition, resulting in elongated tops [7], and only a few are visible after deposition. Especially the much higher Rz values (indicating the maximum height difference between roughness
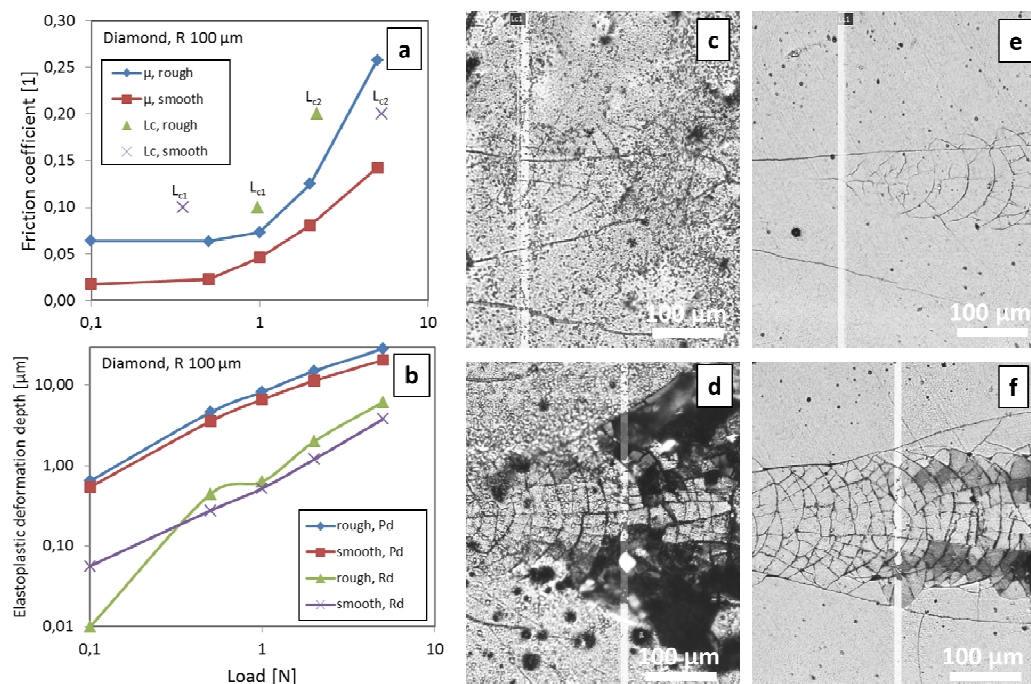

Fig. 1. Results of scratch testing for the smooth and rough coating types on CFRP: (a) Dependency of friction coefficient and critical loads L_{c1} and L_{c2}, (b) elastoplastic (P_d) and plastic (R_d) deformation depth. Light microscopy images of the (c,d) rough and (e,f) smooth coating at (c,e) L_{c1} and (d,f) L_{c2}. Critical loads are indicated by the vertical grey line in the images

tips and grooves) indicate much coarser wrinkle topography of the rougher film, deposited at higher growth rates. Because hardness is a measure of plastic deformation resistance, both the less dense structure due to (healed) cracks and the geometrically easier elastic deformation of a wavy surface are reasons for the lower hardness found for the rougher coating type.

TABLE 1

Thickness, roughness, hardness and elastic modulus for the rough and smooth coating types

	Rough coating	Smooth coating
Thickness [μm]	6.00	6.04
Ra [μm]	1.10	0.99
Rq [μm]	1.47	1.24
Rz [μm]	9.17	7.44
Hardness [GPa]	14.8	15.6
Elastic modulus [GPa]	152	155

Results of scratch testing with progressive load on a HRC indenter are shown in (Fig. 1): The observed critical load L_{c1}, defined by first occurring cracks in the scratch track, was found to be generally higher for the rougher surface, while L_{c2}, leading to coating delamination, is higher for the smoother coating (Fig. 1a). Further, the measured friction coefficients are higher for the rough coating, whereby cohesive fracture in the coating at L_{c1} and adhesive fracture at L_{c2} generally increase friction. The elastoplastic deformation (P_d), indicating the penetration depth of the indenter during scratching, is quite similar for both types. This depth increase is due to crack formation and increased dissipation of normal and shear stress energy at L_{c1} and L_{c2}. Cracks with half-circular shape are generally formed in front of the indenter, where elastoplastic deformation of the substrate piles up material (Fig. 1c-f). Some cracks run straight and parallel to the indentation direction (left to right). The delamination at L_{c2}

leads in the case of the rougher coatings (Fig. 1d) to uncovering of a large area of the substrate, while the delamination is only visible for the smoother coating by a strong tipping of fractured fragments (Fig. 1f).

Tribological properties were tested in reciprocating linear movement mode under high abrasive conditions with Al$_2$O$_3$ balls (Fig. 2), whereby the different loading (2 vs. 5 N) does not affect the friction coefficient (Fig. 2a). However, the behaviour of the smooth coating with low steady-state friction coefficients (~0.08) and the rough coating with constantly increasing friction (up to 0.24 after 1000 contact cycles) is strongly different. Wear of both coatings is similar, as indicated by the measured wear depth (Fig. 2b). Nevertheless, the type of wear is different, independently on the load: For the rough coating (Fig. 2c,e), the sliding occurs predominantly on the wrinkle tops, which results in strong local abrasion (light grey areas). The total removal of the low-friction a-C:H layer on the top is reason for the higher friction coefficients after the run-in period. They lead to higher shear forces and, consequently, parallel cracks in normal direction to the ball movement. The density of the crack network is slightly higher for the higher force conditions (Fig. 2e). Formation of wear debris and increasing scratching by these particles prevents reaching steady-state friction within the tested 1000 cycles. Some of the particles are visible as black dots on the surface. In case of the smooth coating, areal wear occurs instead of local abrasion at wrinkle tops. This is visible by the large, slightly brighter, broad horizontal strip in Fig. 2d. Cracks occur in lower density, but show larger width than for the rough coating. Further, parallel cracks to these cracks occur due to low cycle fatigue, especially for the higher load conditions (Fig. 2f).

Finally, we investigated the wear mechanisms on the micro- to nano-scale on cross-sections for the smooth, ultra-low friction coatings, tested under 2 N normal load (1000 contact cycles) (Fig. 3) and 5 N (100 cycles) (Fig. 4). In both cases,
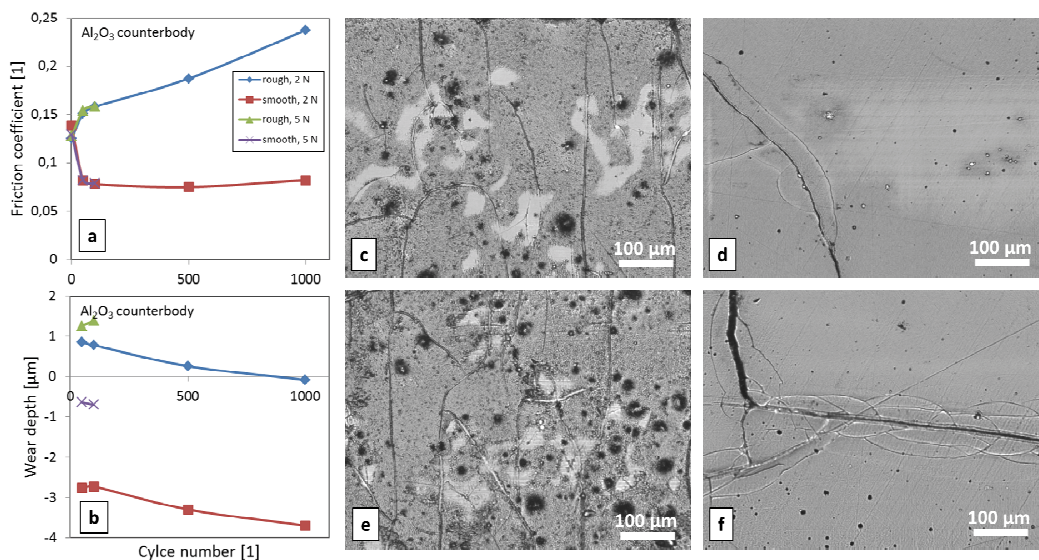

Fig. 2. Tribological testing (reciprocal linear sliding) of the coated CFRP against 6 mm Al$_2$O$_3$ balls: (a) Development of the friction coefficient and (b) the wear depth with the contact cycle number. Light microscopy images of the wear track surfaces (sliding in horizontal direction) for (c,d) 2 N and (e,f) 5 N normal loads. (c,e) Rough and (d,f) smooth coating type
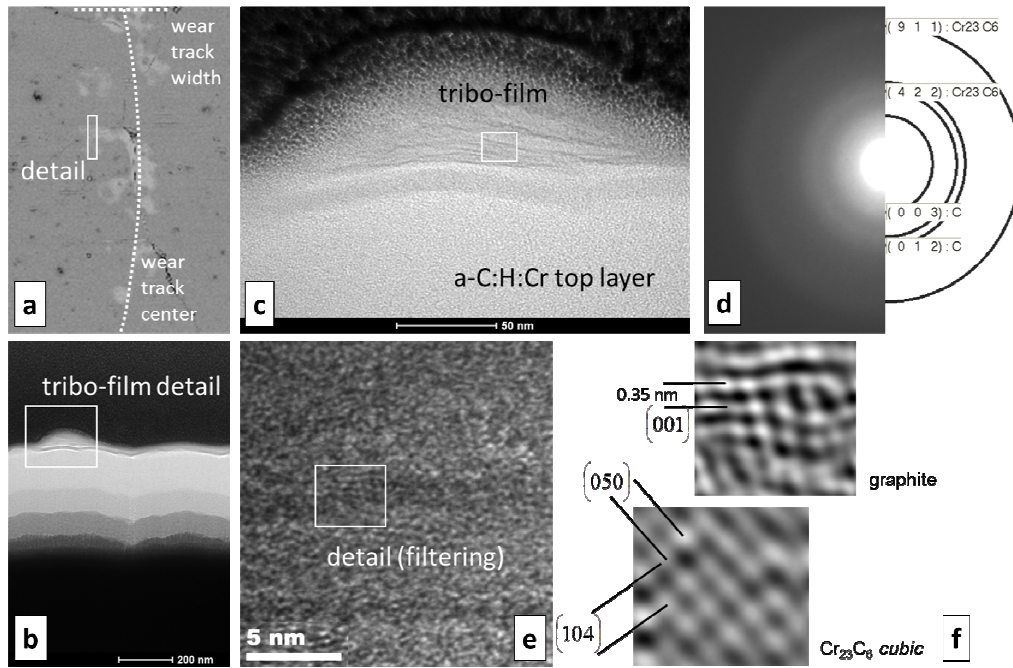
Fig. 3. Detailed investigation of the wear mechanisms of the smooth coating on CFRP after 1000 cycles dry sliding against a 6 mm Al_2O_3 counterpart ball at 2 N normal load: (a) SEM image of the wear track and the position of FIB cutting, (b) TEM cross-section image through the graded top layer a-C:H:Cr coating and (c) HR-TEM image of the adhering tribo-film. (d) Electron diffraction pattern of the tribo-film, and (e) HR-TEM detail within the tribo-film with (f) Fourier transform filtering to determine the occurring phases

FIB cutting was used to cut cross-sections from positions at the boarder of the wear tracks (Fig. 3a and 4a). Additionally to light microscopy, we found both abrasion and tribo-film formation simultaneously. Tribo-films form especially for the 2 N tests (Fig. 3c) on top of the step-wise chemically graded a-C:H:Cr coating (Fig. 3b) and consist of the agglomeration of nanocrystalline C and $Cr_{23}C_6$ phases based on the electron diffraction pattern in FIGURE 3d. The blurred rings indicate close to amorphous structure of this tribo-film, which was proofed by high-resolution imaging (Fig. 3e) and Fourier transform filtering (Fig 3f). Graphite and cubic $Cr_{23}C_6$ were clearly determined in ultra-fine and nano-layered dispersion (Fig. 3e) with only a few nanometers crystal size. Comparing these findings with (Fig. 2a), the ultra-low friction coefficients <0.08 are due to sliding on these tribo-films, which form by micro-abrasion of a-C:H and a-C:H:Cr films at roughness tips, crystallize in the friction heat (as proofed for graphitic C phase) and agglomerate layer-by-layer on nano-scale within the roughness valleys.

In the case of the higher normal load of 5 N, we see both abrasion and cohesive film fraction (Fig. 4a). Cracking is due to too high elasto-plastic deformation of the CFRP substrate (epoxy matrix, as explained above), whereby the coating fractures in tensile stressed regions. These are found in the bent, bulged zones parallel to the counterpart movement at the wear track border, but also perpendicular to the wear track due to low-cycle fatigue. Surely, fracture is influenced by the underlying carbon-fiber - epoxy-matrix microstructure as found in systematic analysis. On the border of the wear track (Fig. 4b), the cracks are only occurring in the a-C:H:Cr top layer, whereby the crack path is strongly influenced by the interfaces between the step-wise chemically graded thin layers (compare to the varying brightness in (Fig. 4b). Tensile stress cracks are switched to shear cracks, oriented parallel to the substrate surface. Although this leads to higher energy dissipation and protection of the underlying a-C:H:Cr and Cr-Cr_2N multilayer coatings, shear cracks lead to delamination of coating fragments from the underneath coating too. This is visible on the left hand side of FIGURE 4b, where a surface-near coating fragment is only loosely bound as seen by the cracks on 3 sides. Also the darker region in (Fig. 4a) below the "detail b" mark indicate spallation of a-C:H:Cr top layer. In the wear track centre, deeper fracture is evident, which reaches the Cr-Cr_2N multi-layered base layer (Fig. 4c). Higher Hertzian contact pressure results in more intensive abrasion as visible by the worn coating part on the upper right hand side at the crack start too. Nevertheless, crack arrest mechanisms in the Cr-Cr_2N multi-layered coating switches crack propagation from normal direction to the parallel, shear direction. Finally, the crack arrests within the coating without any large coating spallation. Different mechanical properties of the Cr and Cr_2N layers lead to plastic shear deformation under 45° and brittle fracture within the formed deformation band (Fig. 4d). In combination with results in (Fig. 2), it can be stated finally, that 100 cycles sliding of the Al_2O_3 ball under 5 N normal force (which are normal test conditions for coated mild steels) does not destroy the coating on soft CFRP in such a manner, that the low friction properties are lost. Consequently, such smooth multilayer coatings provide both low-friction behaviour for dry sliding at medium load in mechanical engineering as well as safety in overload events.
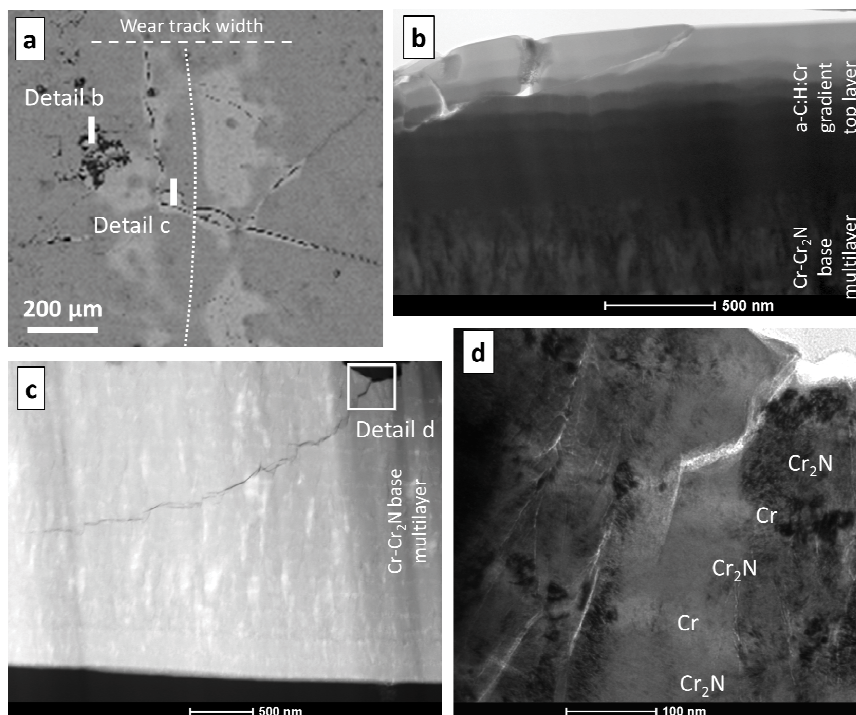
Fig. 4. Detailed investigation of the wear mechanisms of the smooth coating on CFRP after 100 cycles dry sliding against a 6 mm Al_2O_3 counterpart ball at 5 N normal load: (a) SEM image of the wear track and the positions of FIB cutting for details in (b-d). Cross-section TEM images (b) at the boarder of the wear track with fracture of the graded a-C:H:Cr layer coating and (c) in the wear track centre with abrasive wear of the a-C:H:Cr and the top part of the $Cr-Cr_2N$ multilayer coating and further crack propagation. (d) HR-TEM detail of the fracture mechanisms with brittle cracking and plastic shearing within the $Cr-Cr_2N$ multilayer

4. Conclusions

CFRPs excel by their very high specific strength, which opens a wide field in ultra-light weight design. Nevertheless, the fibre reinforcement results in strong orientation dependency of mechanical and thermal properties. Further, the combination of soft epoxy matrix and embedded high strength fibres offers only low tribological resistance in sliding contacts. Thus, wear protection by hard coatings is the only option to functionalize these construction materials. The low load support of the epoxy matrix requires tough materials, preventing crack propagation through the whole coating during local overloading. This was realized in this work by a magnetron sputtered, multi-layered design of hard chromium nitride layers in between soft, deformable chromium layers. A chemically graded design provides high toughness for the low-friction diamond-like carbon top layer. In tribological testing under high Hertzian pressure, we found a strong influence of roughness on the tribological performance (friction coefficient, wear rate) as well as adhesion. Origin of the roughness variation at the similar CFRP substrates was a different deposition rate, leading to higher temperature load on the substrates during deposition. Resulting thermal expansion of the epoxy matrix on the micro scale leads to a wavy, wrinkled surface topography with higher amplitude for ~20°C higher surface temperature at the end of the deposition for higher rate conditions. Scratch testing revealed for the rougher coating higher cohesive strength in the film, but lower adhesive strength on the CFRP. Both in scratch testing as well as in reciprocal sliding testing against alumina balls, the friction coefficients are lower for the smooth coatings. Tribology is dominated by abrasion by Al_2O_3, whereby lower normal loads trigger the abrasion on nanoscale and the agglomeration of nano-layered, nanocrystalline, ultra-low-friction tribo-films, while higher loads results in coating fracture after overloading, but even in this case low friction behaviour.

REFERENCES

[1] S. Guanhong, H. Xiaodong, J. Jiuxing, et al., Applied Surface Science **257**, 7864 (2011).

[2] S.M. Vyawahare, Doctoral dissertation, Wichita State University (2006).

[3] L. Di, B. Liu, J. Song, et al., Applied Surface Science **257**, 4272 (2011).

2151

[4] Y.S. Lin, C.H. Hu, C.A. Hsiao, Composites Science and Technology, **71**, 1579 (2011).

[5] M. Stueber, H. Holleck, H. Leiste, et al., Journal of Alloys and Compounds **483**, 321 (2009).

[6] J.M. Lackner, W. Waldhauser, P. Hartmann, et al., Thin Solid Films **520**, 2833 (2012).

[7] J.M. Lackner, W. Waldhauser, C. Ganser, et al., Surface and Coatings Technology **241**, 80 (2014).

[8] J.M. Lackner, L. Major, M. Kot, et al., Bulletin of the Polish Academy of Sciences: Technical Sciences **59**, 343 (2011).

[9] J.M. Lackner, W. Waldhauser, B. Major, et al., Thin Solid Films **534**, 417 (2013).

[10] J. Robertson, Materials Science and Engineering, R: Reports **37**, 129 (2002).

[11] A. Grill, Diamond and related materials **8**, 428 (1999).

[12] H. Ronkainen, S. Varjus, J. Koskinen, et al.. Wear **249**, 260 (2001).

[13] Y. Liu, A. Erdemir, E.I. Meletis, et al., Surface and Coatings Technology **82**, 48 (1996).

[14] Y. Pauleau, F. Thiery, Surface and Coatings Technology **180**, 313 (2004).

[15] Y. Pauleau, F. Thiery, V. Uglov, et al., Surface and Coatings Technology **180**, 102 (2004).

[16] H. Dimigen, H. Hübsch, R. Memming, R.. Applied Physics Letters **50**, 1056 (1987).

[17] V.V. Uglova, V.M. Anishchik, Y. Pauleau, et al., Vacuum **70**, 181 (2003).

[18] C.A. Charitidis, International Journal of Refractory Metals and Hard Materials **28**, 51 (2010).

[19] J.M. Lackner, W. Waldhauser, M. Schwarz, et al., Vacuum **83**, 302 (2008).

[20] J.M. Lackner, W. Waldhauser, L. Major, et al., Computational and Structural Biotechnology Journal **6**, 1 (2013).